Electron Acceleration in the Force-Free Corona by Dissipative Electric Fields: a 'Global' Flare Simulation

Kaspar Arzner (PSI) and Loukas Vlahos (AUTH)

thanks to: M. Georgoulis, E. Rantsiou

CONTENT

- Physical Considerations; Acceleration Mechanism
- Modeling of Generic Coronal Fields
- Particle Orbits
- Observational Predictions (HXR, Radio)

1 Physical Considerations

- Solar flares seem to be ‘catastrophic’ events, where structurally stored magnetic energy B^2 is converted into other forms, and, ultimately, into heat.
- The underlying physics is likely to be *irreversible* and *dissipative*; a Hamiltonian might not exist.
- From a macroscopic point of view, Poynting’s theorem

$$\frac{\partial U}{\partial t} + \nabla \cdot \mathbf{S} = -\mathbf{j} \cdot \mathbf{E} \tag{1}$$

  requires $\mathbf{j} \cdot \mathbf{E} > 0$ whenever electromagnetic energy $U = \frac{1}{2}(E^2 + H^2)$ is converted into some other form of energy (and not just exported by the Poynting flux $\mathbf{S} = \mathbf{E} \times \mathbf{H}$).
- It is thus tempting to localize particle acceleration in regions where $\mathbf{j} \cdot \mathbf{E} > 0$.
- The nonlinear MHD equations tends to align $\mathbf{B}$ with $\mathbf{u}$ (Alfvén effect), and, primarily, $\mathbf{j}$ with $\mathbf{B}$. Thus $\mathbf{j} \cdot \mathbf{E} > 0$ implies $\mathbf{B} \cdot \mathbf{E} \neq 0$.
- The (macroscopic) parallel electric field usually compensates for Coulomb drag, but balance depends on velocity. Runaway in twisted flux tubes.

2 Simulation Strategy, Outline

- Consider electrons in a slab $0 < z <$ H filled with generic coronal fields

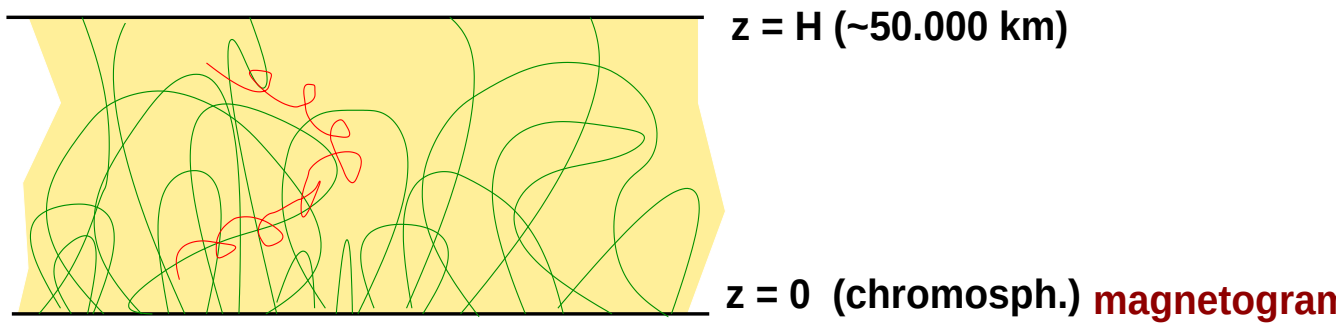

- Field construction: force-free extrapolation of SOHO magnetograms, plus (slight) randomizing of the wave vectors to avoid periodic continuation
- Time-independent fields (over a few s), $\mathbf{E} = \eta \mathbf{j}$ with η = 0 or $\eta > \eta_{\mathrm{Spitzer}}$.
- Super-Dreicer electrons are treated as collisionless test particles
- Avoiding large but passive arrays $\longrightarrow$ sparse-Fourier representation, local computation of $\mathbf{B}(\mathbf{x})$ and its derivatives
- Gyrokinetic approximations where applicable
- Start all particles at t = 0, and compute chromospheric impact (HXR lightcurve, spectrum) and radio emissions. Explore the effect of field parameters.

3 Boundary Conditions

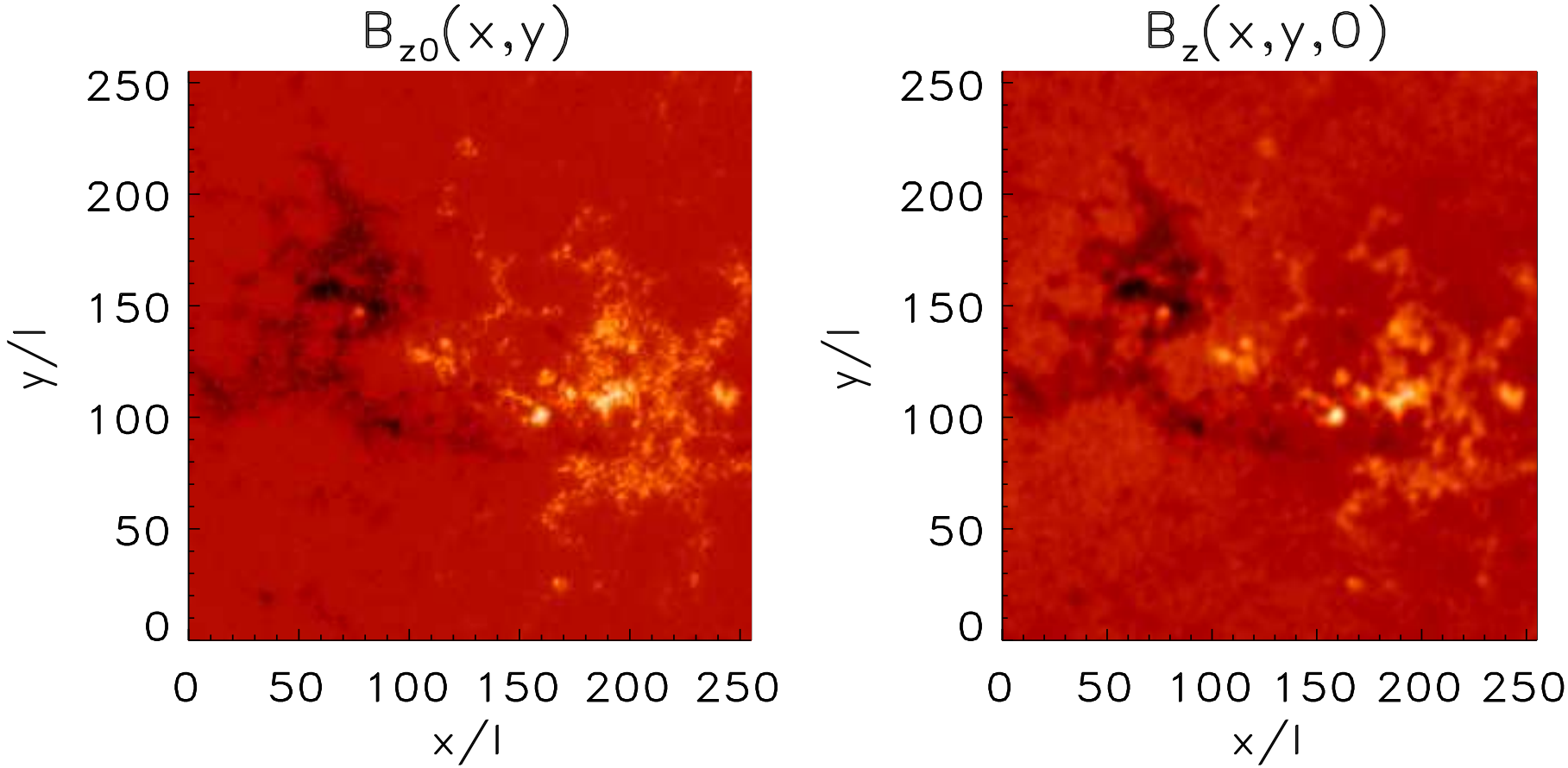

Left: SOHO/MDI magnetogram recorded on Aug 17, 2002, 10:40 UT. The image centre is at (200”,70”) with l = 1.95”. Right: its sparse-Fourier representation.

4 Sparse-Fourier Sampling

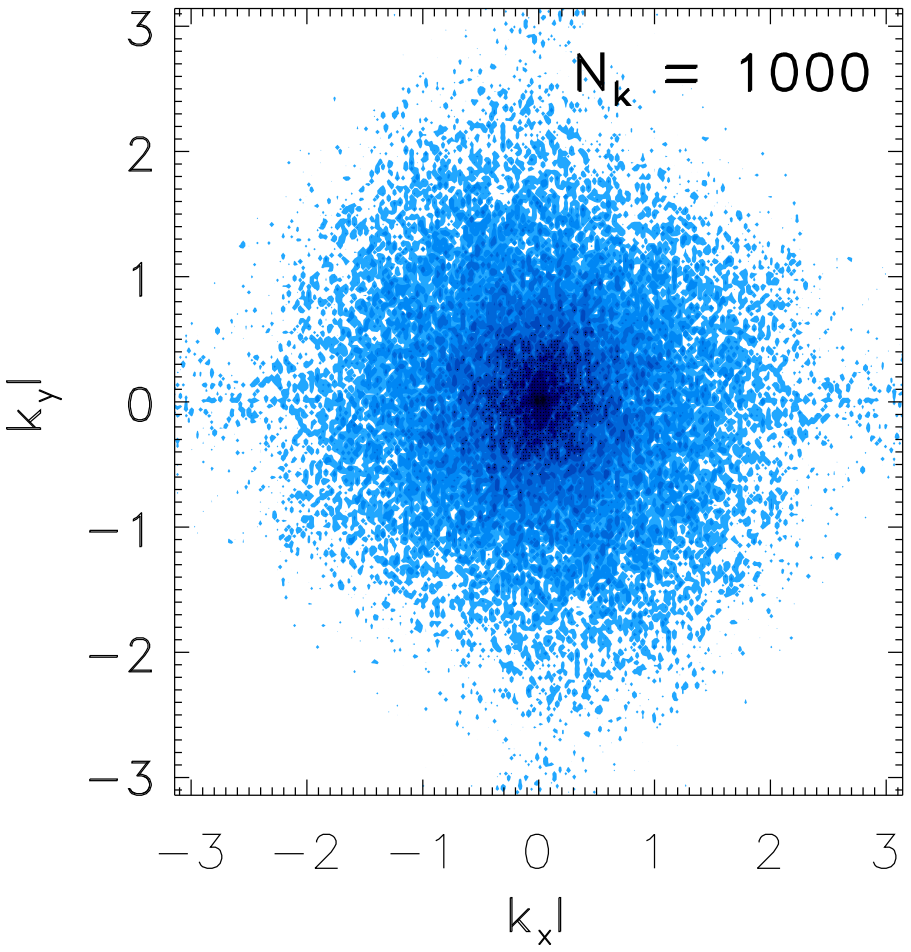

PROCEDURE:

- Take the FFT of the longitudinal SOHO magnetogram
- Select those N_k wave vectors (black dots) with largest power spectral density (blue color)
- Randomize the $\mathbf{k}$'s to avoid periodic continuation ($\Delta\mathbf{k} \ll 2\pi/N$ with N = 128 or 256 the magnetogram size)

5 Force-Free Extrapolation ($\nabla \times \mathbf{B} = \alpha \mathbf{B}$)

Assuming constant α, the force-free condition implies $|\mathbf{k}|^2 = \alpha^2$. Fitting the z-components of the eigenvectors $\mathbf{b}(\mathbf{k})e^{i\mathbf{k}\cdot\mathbf{x}}$ at z = 0 to the magnetogram yields

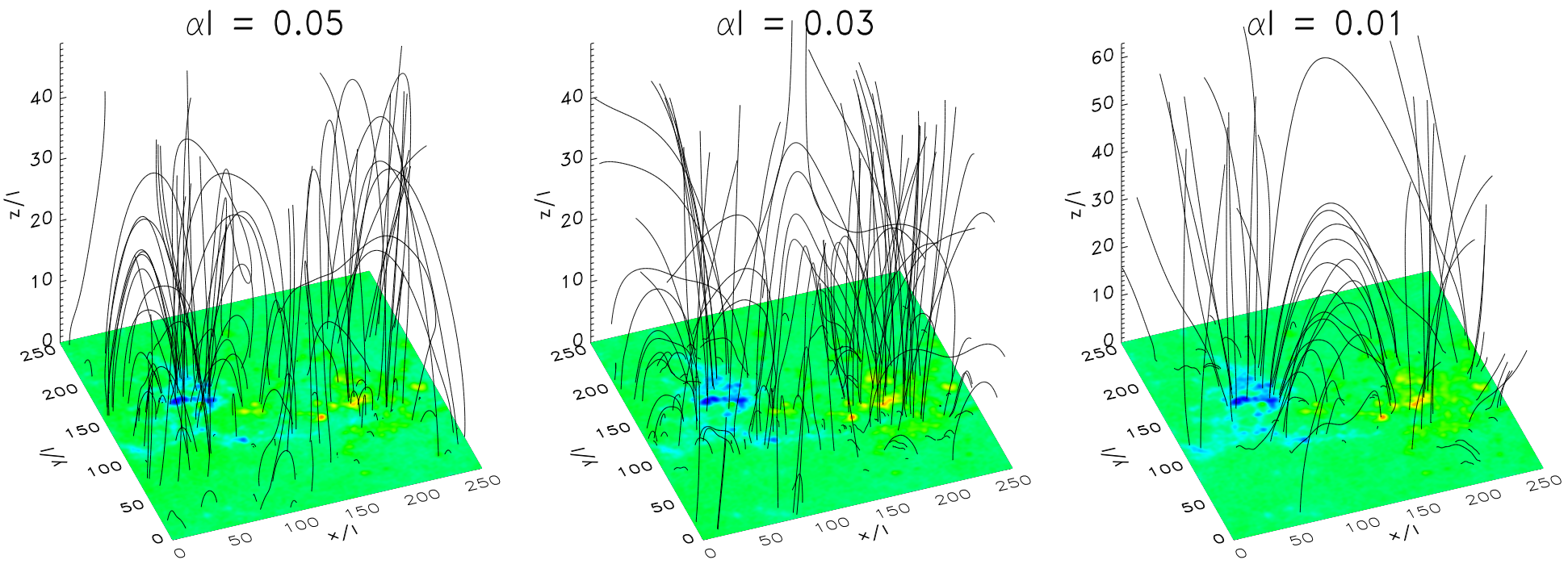

The shown fieldlines start at z = 0 at random with density $\propto |\mathbf{B}(x, y, 0)|$. The majority (>99%) of used modes decays with height (Im $k_z > 0$). Small scales decay more rapidly; the largest decaying scale is $2\pi/\alpha$.

6 Anomaleous Resistivity η and Dissipative Field $\mathbf{E} = \eta\mathbf{j}$

Several criteria (drift wave- or MHD kink instabilities, qualitative non-linear arguments) for the occurrence of anomaleous resistivity have been proposed; but no general and rigorous results seem available. Two plausible criteria are:

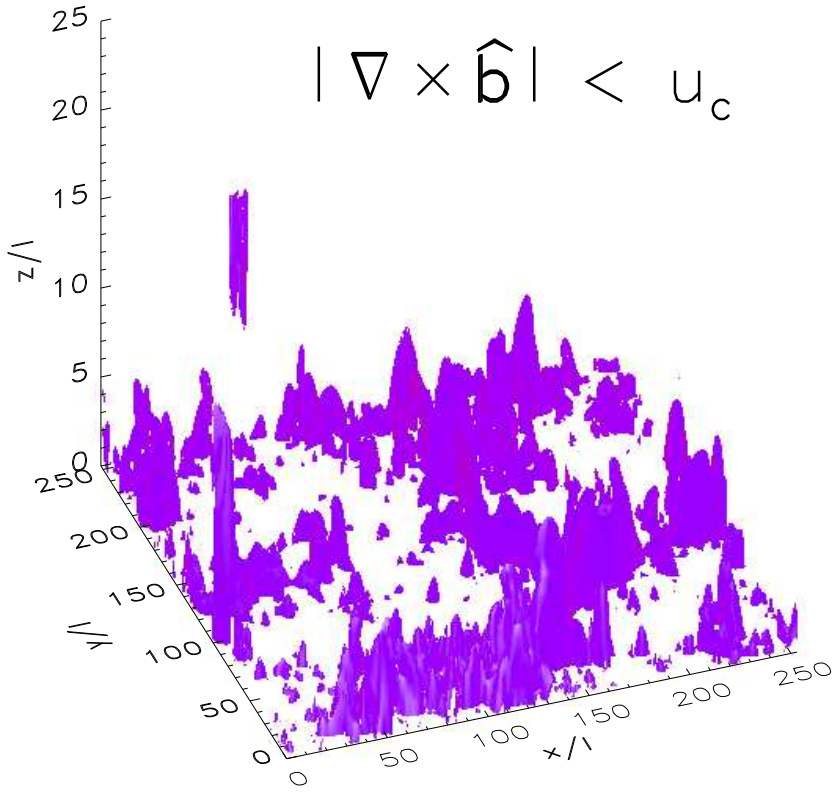

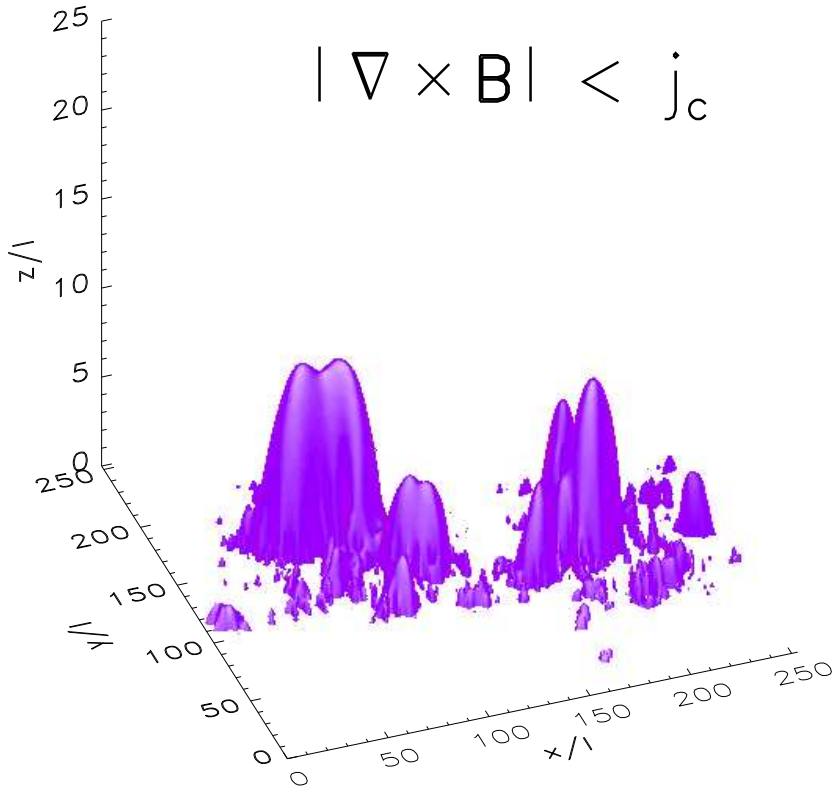

We use here the twist threshold (left, $\hat{\mathbf{b}} = \mathbf{B}/|\mathbf{B}|$), motivated by Parker's critical angle. Our u_c corresponds to a twist scale $1/u_c \sim$ 3000 km. Inside the violet regions, $\eta > 0$ and $\mathbf{E} = \eta\mathbf{j}$ exceeds E_D by about one magnitude. By the force-free assumption $\mathbf{j} = \alpha\mathbf{B}$ with $\alpha > 0$, $\mathbf{E}$ is *parallel*.

7 Particle Orbits (and Unit Conventions)

The exact equations of motion are $d\mathbf{x}/dt = \mathbf{v}$ and $d(\gamma\mathbf{v})/dt = \mathbf{E} + \mathbf{v} \times \mathbf{B}$. The gyrokinetic approximation used here is (Littlejohn 1981,1982; Brizard 1999):

$$\begin{aligned} \frac{d\mathbf{X}}{dt} &= \frac{1}{B_{\|}^{*}}\Big(\frac{p_{\|}}{\gamma}\mathbf{B}^{*} + \frac{\mu}{\gamma}\hat{\mathbf{b}} \times \nabla B - \hat{\mathbf{b}} \times \mathbf{E}^{*}\Big) \\ \frac{dp_{\|}}{dt} &= -\frac{1}{B_{\|}^{*}}\mathbf{B}^{*} \cdot \Big(\frac{\mu}{\gamma}\nabla B - \mathbf{E}^{*}\Big) \end{aligned}$$

with $\mu = \frac{1}{2}\gamma^2 v_{\perp}^2/B$ (conserved), $\gamma^2 = 1 + p_{\|}^2 + 2\mu B$, $\mathbf{B}^{*} = \mathbf{B} + p_{\|}\nabla \times \hat{\mathbf{b}}$, and $\mathbf{E}^{*} = \mathbf{E} - p_{\|}\partial\hat{\mathbf{b}}/\partial t$. The gyro phase Θ is subject to gauge freedom and obtained from the parallel transport (Fermi-Walker) equation (Littlejohn 1988)

$$\frac{d\hat{\mathbf{e}}}{ds} = -\hat{\mathbf{b}}\Big(\frac{d\hat{\mathbf{b}}}{ds} \cdot \hat{\mathbf{e}}\Big) \tag{2}$$

where s is the distance along the gyrocenter orbit and $\hat{\mathbf{e}}(0)$ is a unit vector along the initial Larmor radius. All electrons start out at t = 0 with v_0 = 0.1c in random direction, uniformly distributed inside the dissipation regions.

8 Regime switching and Accuracy Control

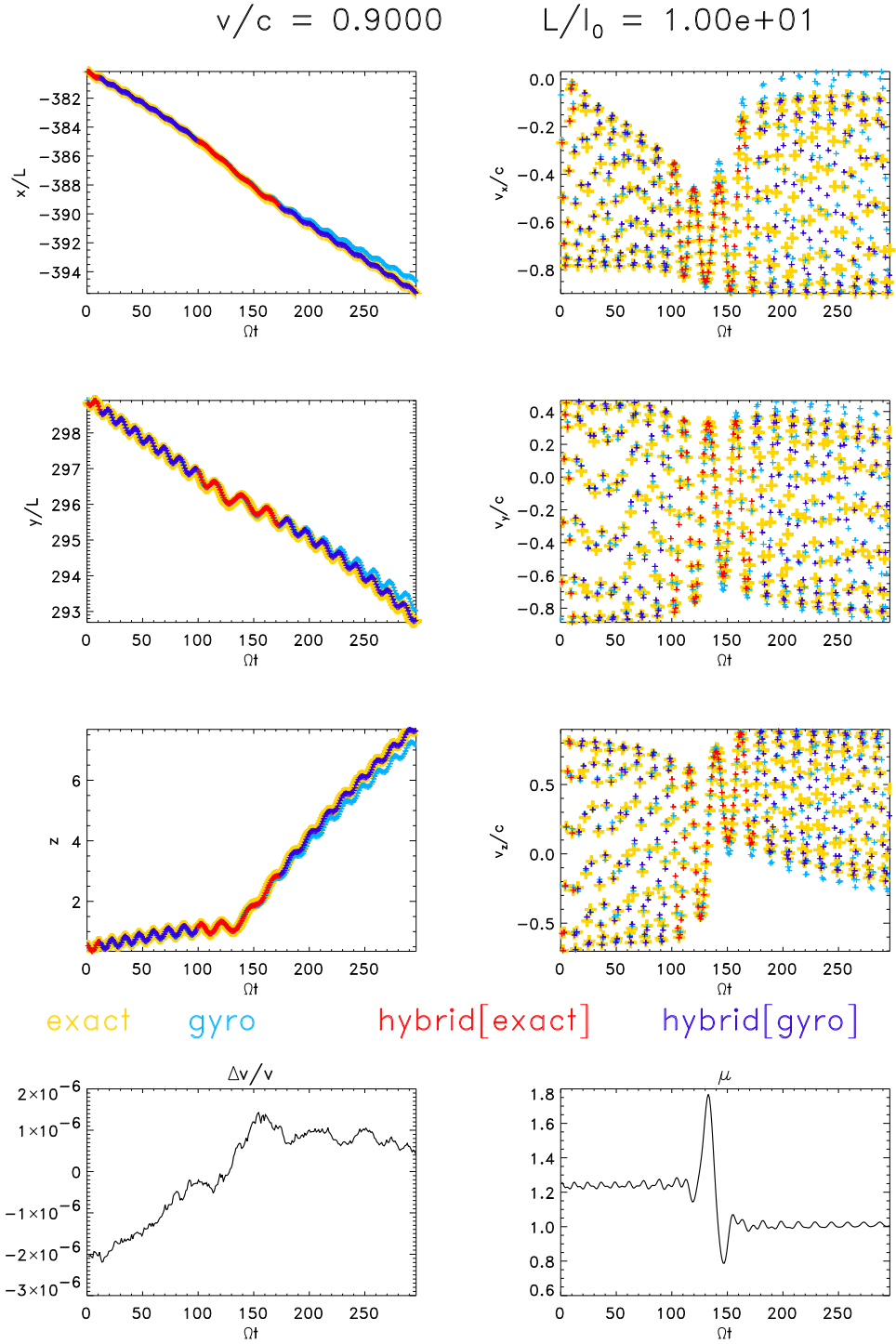

- Left: benchmark orbit. The time unit is Ω^{-1} with $\Omega^2 = \frac{1}{2}\sum_{\mathbf{k}} |\mathbf{b}(\mathbf{k})|^2$ the mean square chromospheric gyro frequency.
- Both exact and gyrokinetic orbits are integrated using Cash/Karp RK4/5. The time step is adapted to ensure $\Delta x/l < 10^{-6}$ and $\Delta p/p_0 < 10^{-9}$.
- The fields are evaluated at a lower rate, linearly extrapolated from gradients, and updated if $|\partial B \cdot (\mathbf{x} - \mathbf{x}_{\rm old})|/B > \epsilon_B$ with $\epsilon_B = 10^{-3}$.
- Hybrid mode: exact orbit tracking is enforced if $\rho^2 \sum_{ij} |\partial_i B_j|^2 > \epsilon_g^2 B^2$ with $\rho = |\mathbf{p}|/B$ and $\epsilon_g = 0.05$

9 Observational Diagnostics

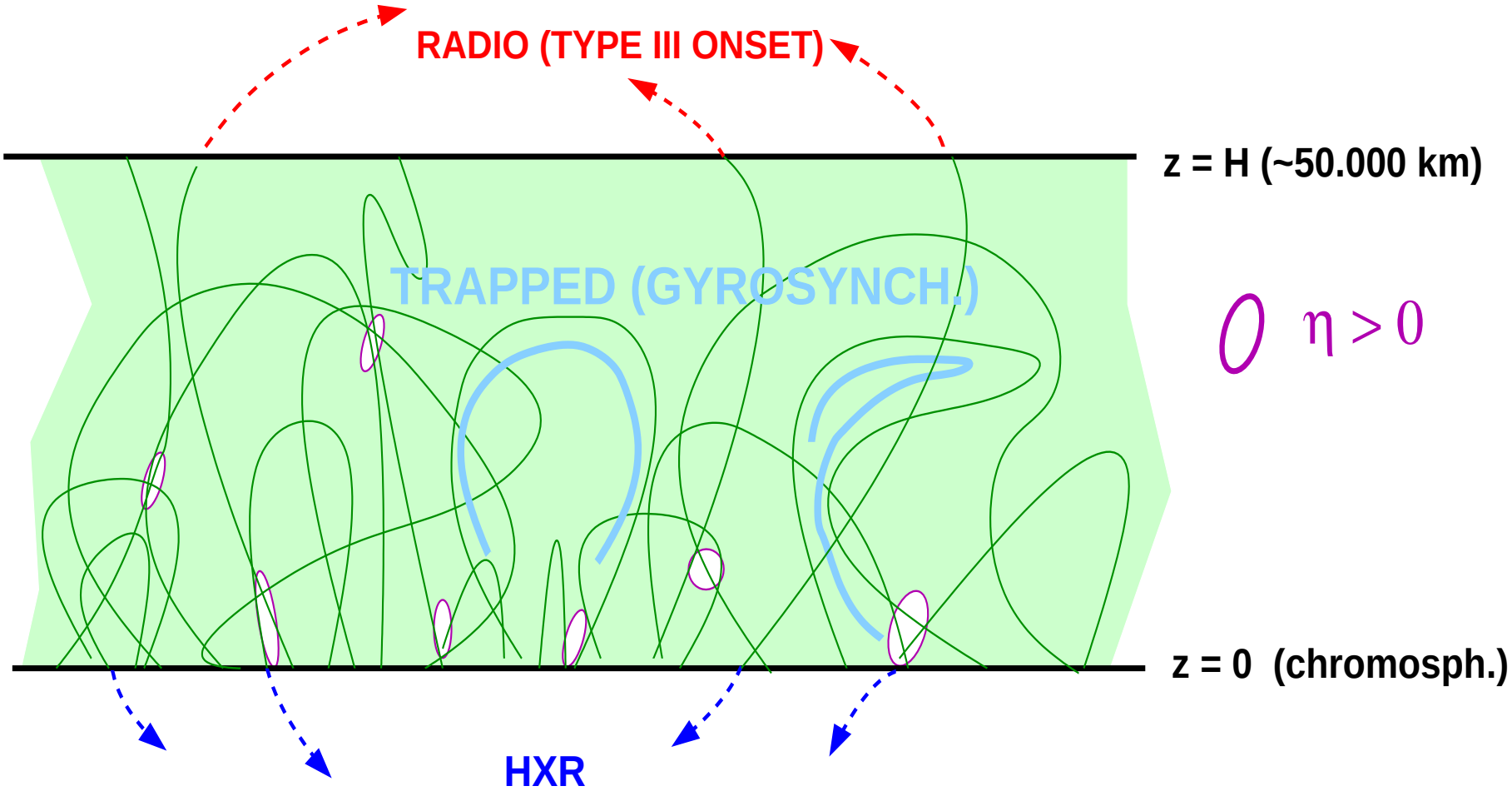

Electrons leaving the simulated slab at z = 0 are associated with HXR; electrons leaving at z = H, with (normal drifting) type III onsets. Trapped electrons are associated with gyrosynchrotron radiation.

10 Precipitating, Escaping and Trapped Electrons

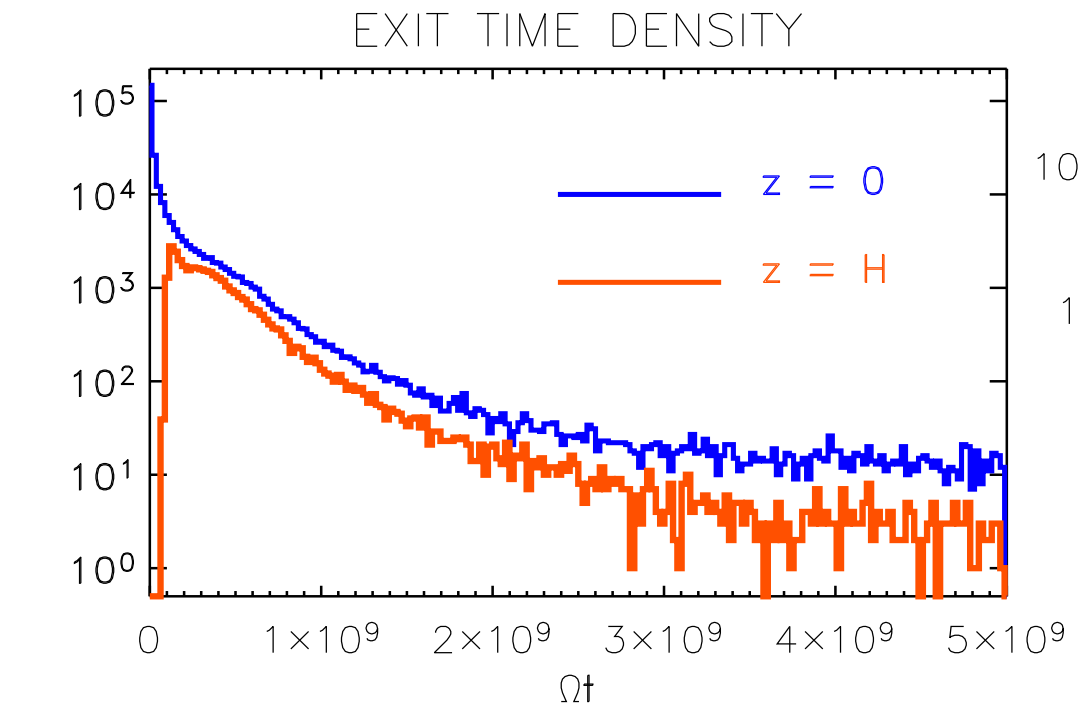

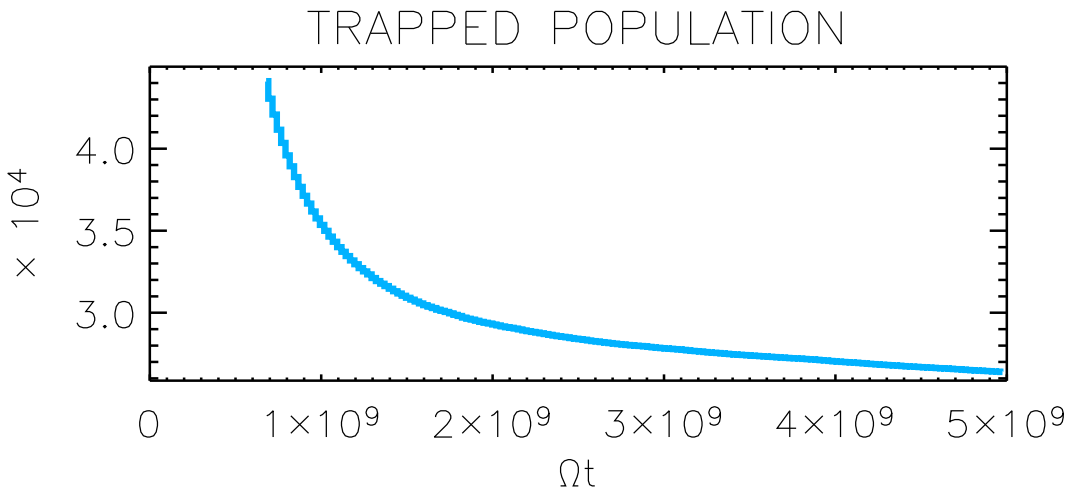

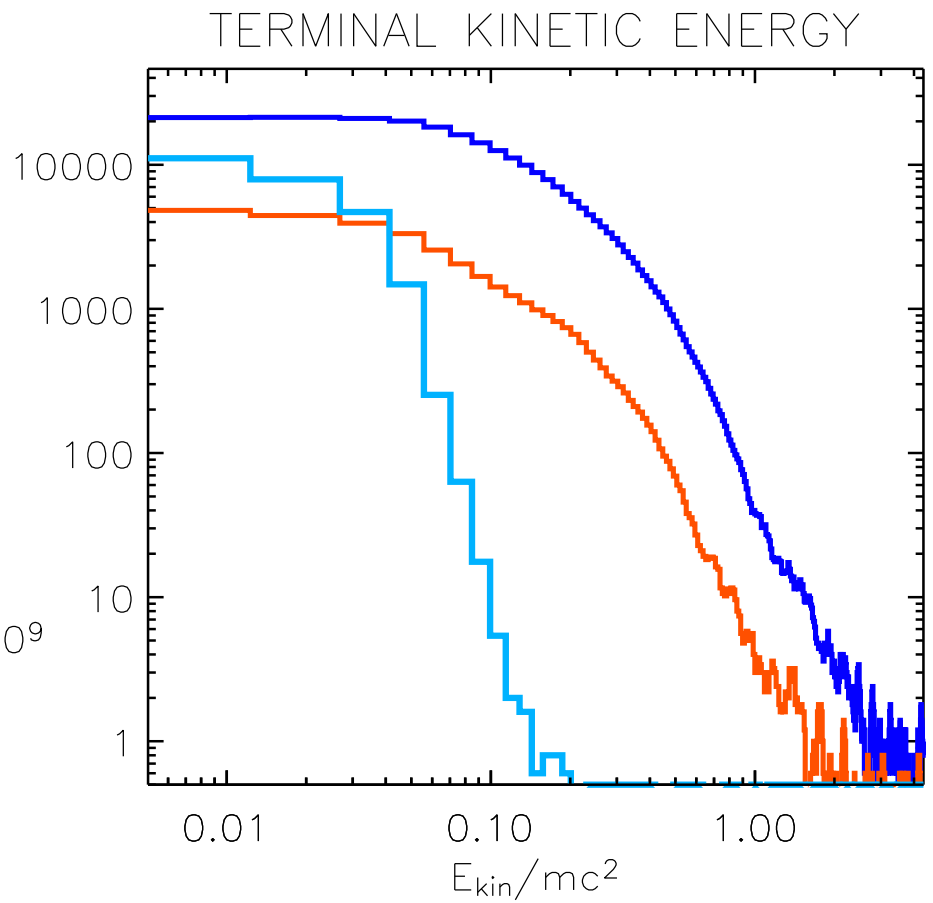

u_cl = 0.20
αl = 0.03
η = 6.84

Example simulation with $3 \cdot 10^5$ particles. mc^2 = 511 keV; $\Omega t = 10^9$ corresponds to about 1s in real time (B = 60 G).

11 Predicted Impact (HXR) Map

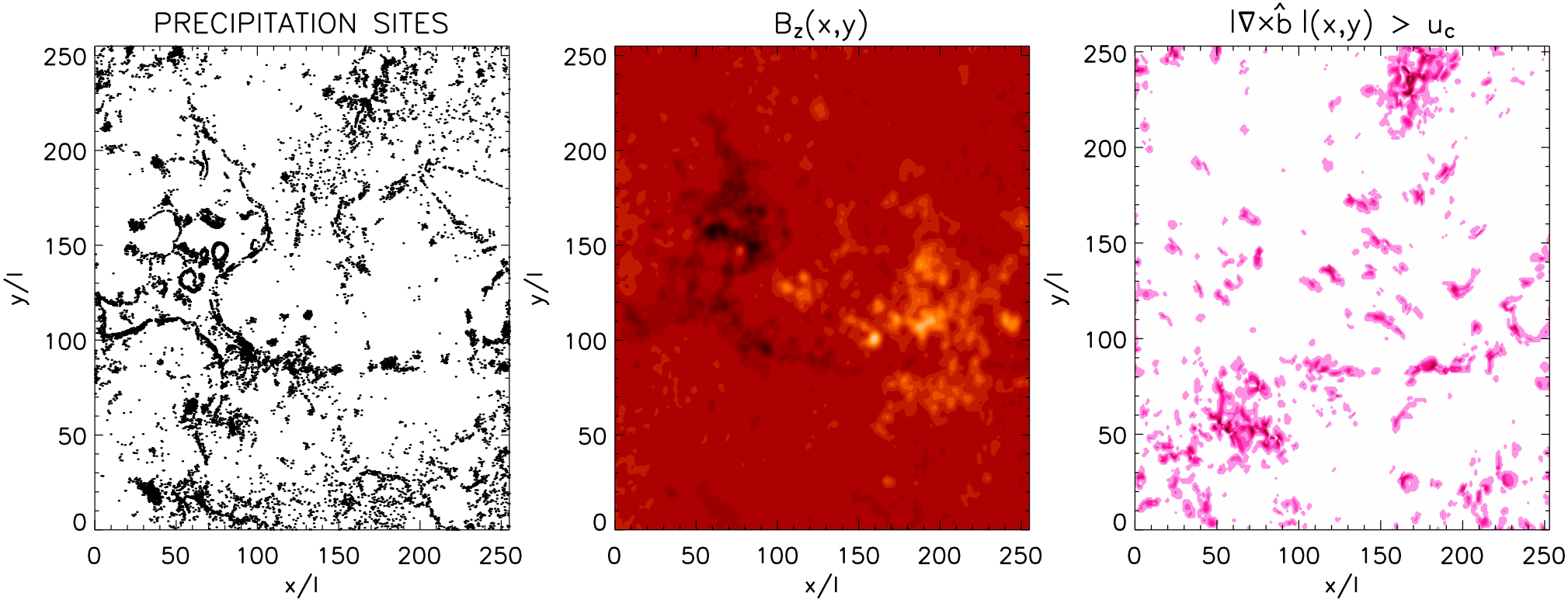

Absolute scaling: $l \sim 1$". Few impacting particles at positive polarity ($B_z > 0$) because of the assumption $\alpha > 0$.

The impact map will provide a straightforward experimental test when compared with RHESSI pictures!

12 HXR and Radio Light Curves, Electron Spectral Evolution

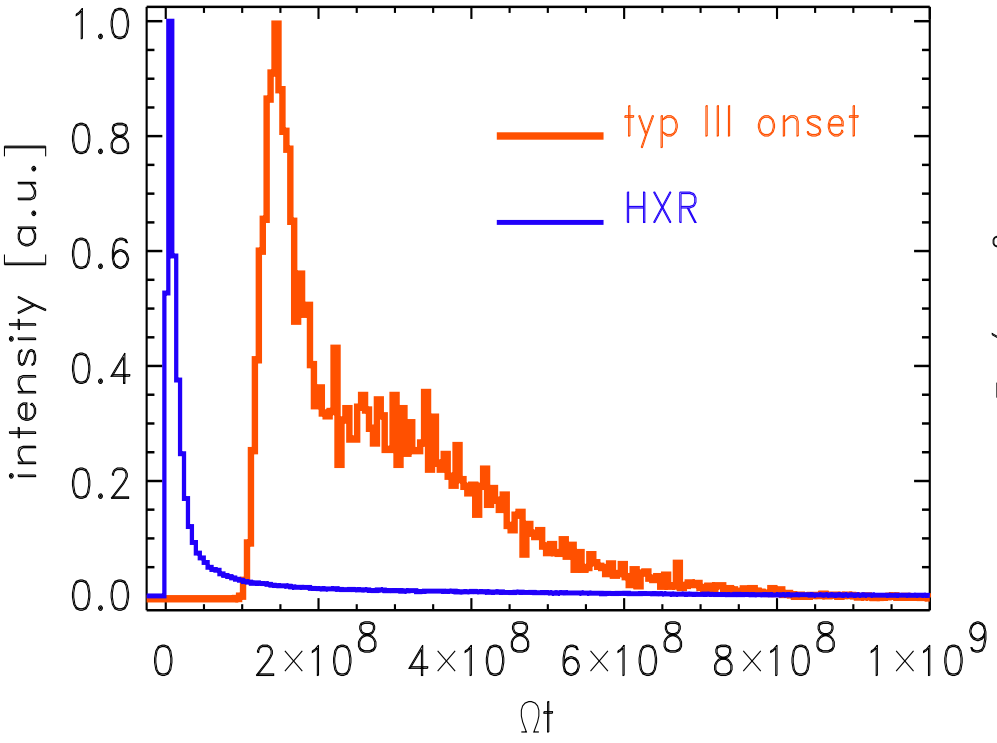

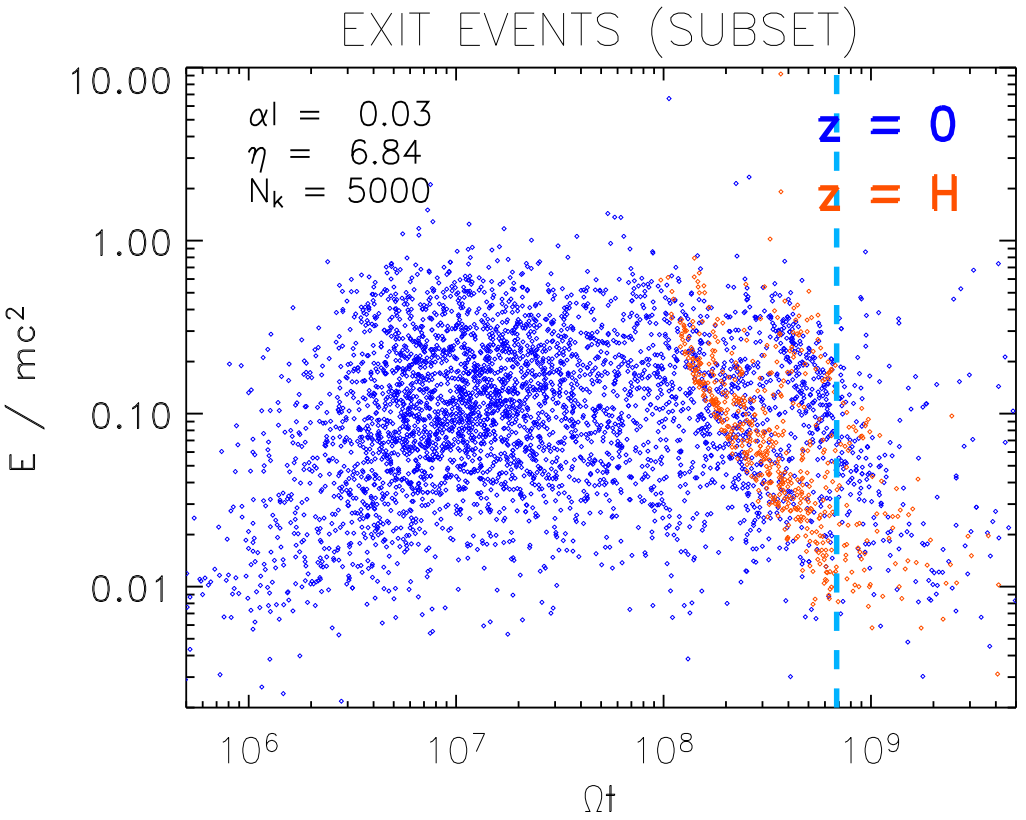

Light curves assume that $F_{\rm HXR} \propto \dot{N}_0$ (incoherent) and $F_{\rm radio} \propto \dot{N}_H^2$ (coherent), with $\dot{N}_0$ and $\dot{N}_H$ the exit rates at z = 0 and $z = H$, respectively. Since the numbn-ert of test particles and the background density are unspecified, the intensities and radio frequency $\gtrsim f_p$ are arbitrary. Typically, $f_p \sim$ 200 MHz.

13 HXR Spectrum (Thick-Target Bremsstrahlung)

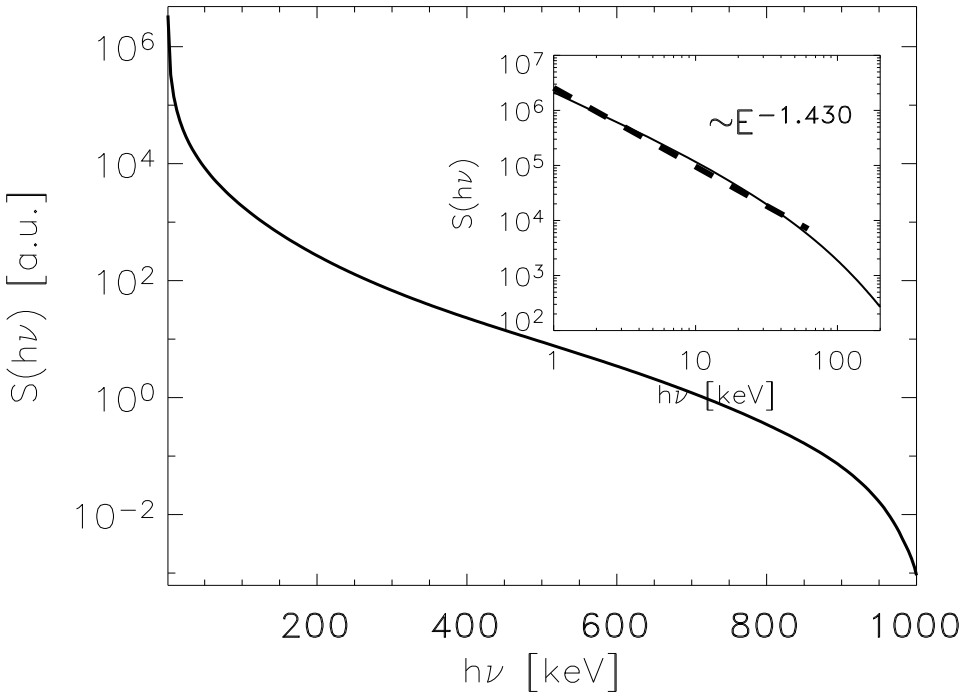

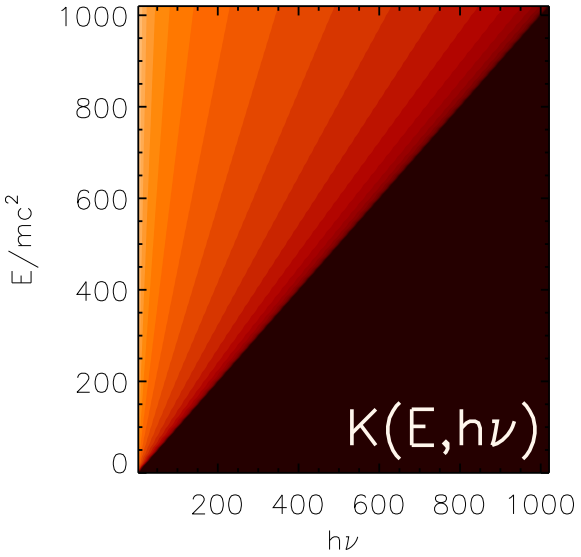

The HXR spectrum $S(h\nu)$ is obtained from the electron spectrum $f(E)$ by

$$S(h\nu) = \int_{h\nu}^{\infty} K(E, h\nu) f(E)\, dE$$

with kernel

$$K(E, h\nu) = \int_{h\nu}^{E} \sigma(E', h\nu) \frac{v'}{\dot{E}'}\, dE'$$

where $\sigma(E, h\nu)$ is the Bethe-Heitler cross section [general relativistic case, Koch & Motz (1959) 3BN, incl. Elwert's Coulomb screening], and assuming that $\dot{E} \propto v/E$ (Brown, 1971).

14 Gyrosynchrotron Spectrum (Optically Thin for Simplicity)

Each electron emits at frequency $\omega = n\Omega/\gamma$ with intensity (Schott, 1912)

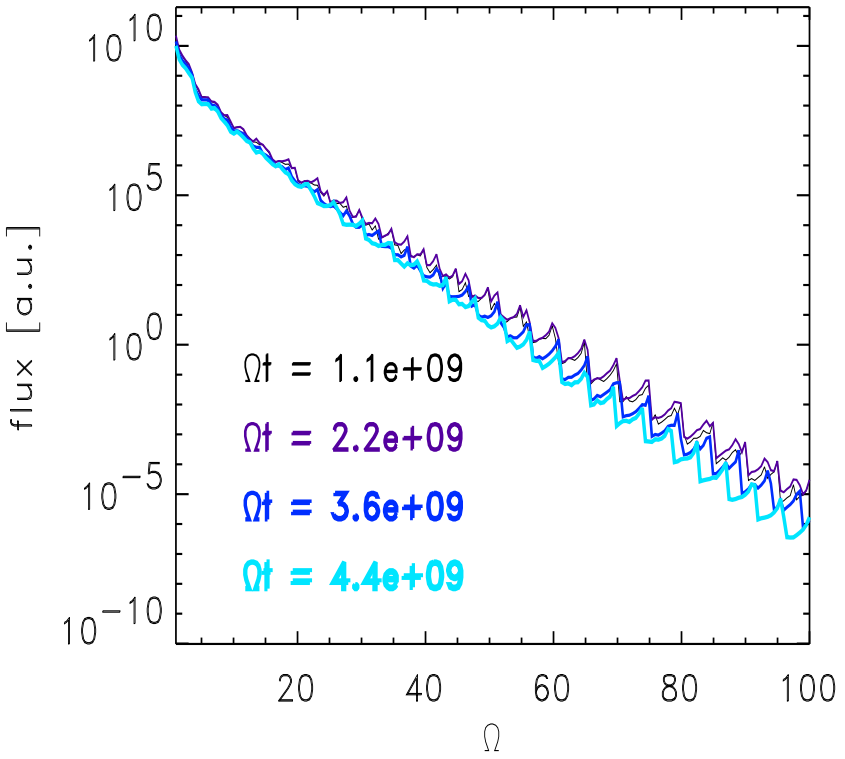

$$\frac{n^2\Omega^2}{\gamma^2}\left(\tan^2\theta\ J_n^2(nv\cos\theta) + v^2 J_n'^{\,2}(nv\cos\theta)\right)$$

$$\simeq \frac{\Omega^2}{\gamma^2}\frac{1+\sin^2\theta}{\cos^2\theta}\frac{n}{2\pi}\left|\frac{ev\cos\theta}{2}\right|^{2n} \quad (v<1),$$

where e = 2.718 and $0 < \theta < 90^o$ is the angle between the gyration plane and the line of sight (0,0,1). Left: numerical superposition of the trapped population ($v \lesssim$ 0.4).

Since $\gamma \gtrsim 1$, the spectrum is dominated by the distribution of $\Omega = eB/m$ and by the (exponential) decay of high harmonics ($n > 10$). Using B=60G from SOHO/MDI, $\Omega = 1$ corrsponds to 170 MHz.

15 Parameter Exploration ($u_c l$=0.2)

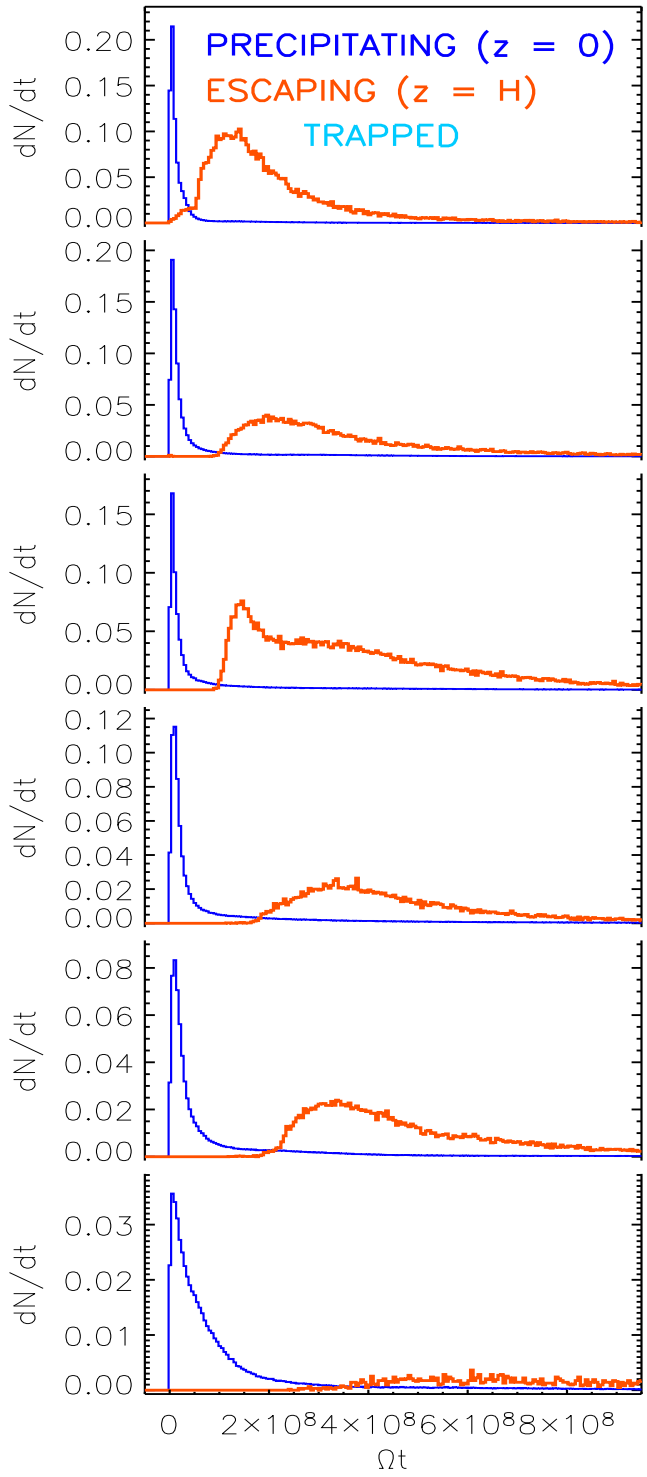

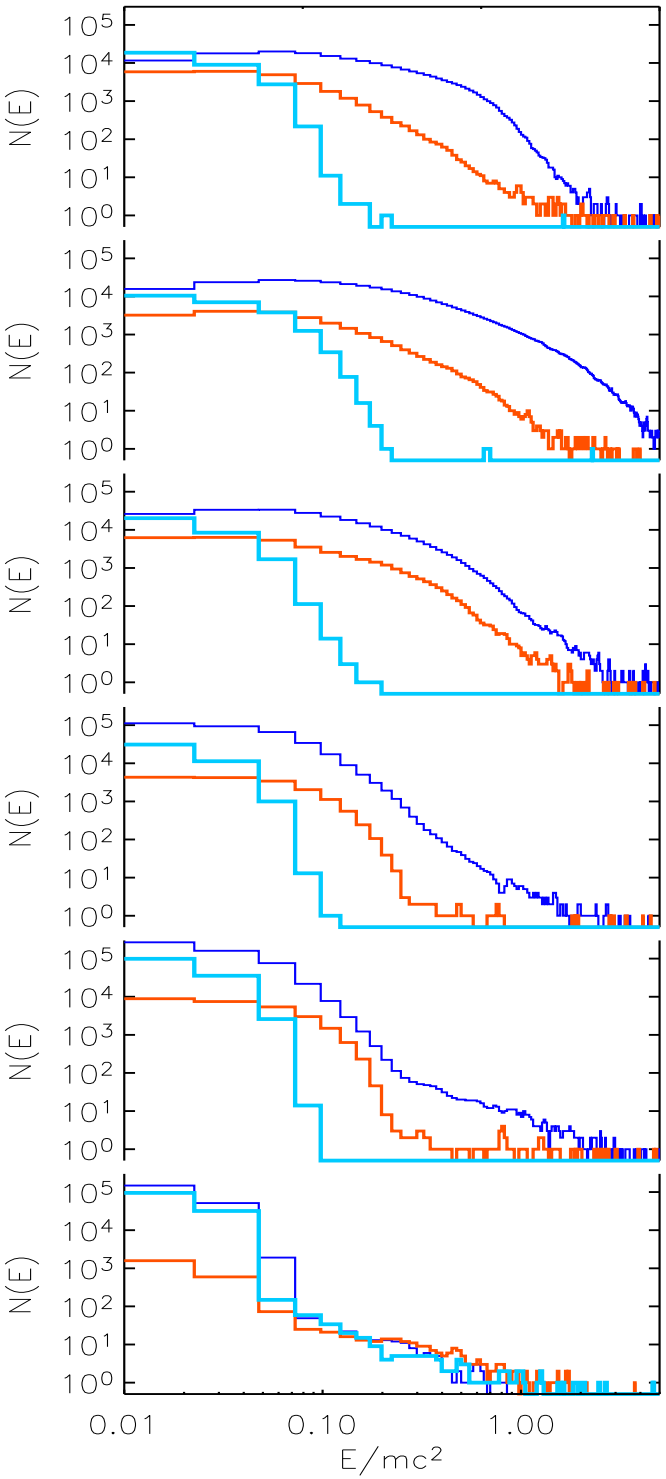

αl = 0.05
η = 4.38
N_k = 5000

αl = 0.05
η = 6.84
N_k = 5000

αl = 0.03
η = 6.84
N_k = 5000

αl = 0.01
η = 6.84
N_k = 5000

αl = 0.01
η = 6.84
N_k = 1000

αl = 0.01
η = 1.37
N_k = 1000

16 Distribution of (terminal) Particle Energy and 'Voltage Drops'

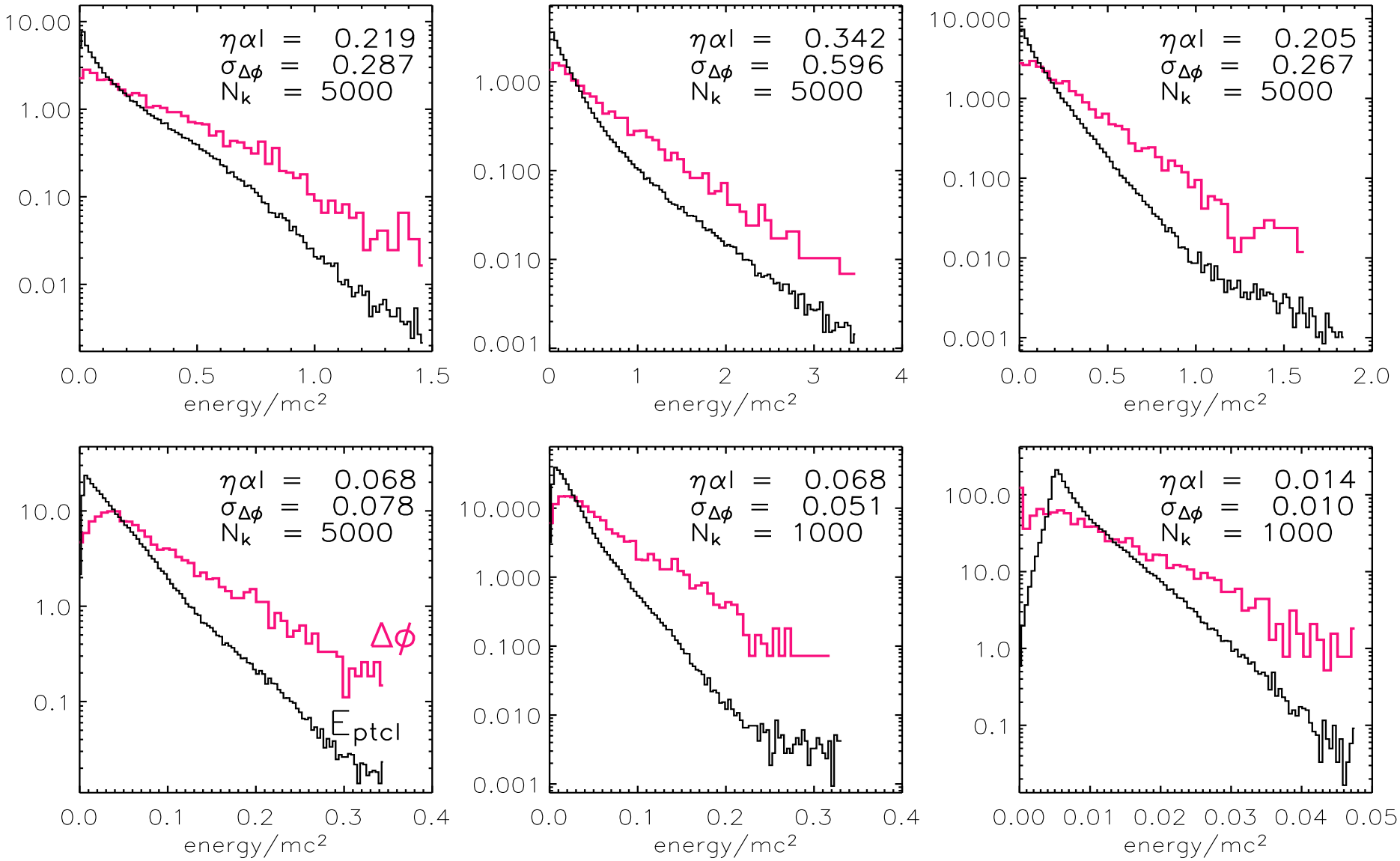

$\Delta\phi \doteq \int \mathbf{E}\cdot d\mathbf{l} = \eta\alpha \int B\, dl$ along a magnetic field line segment intersecting the domain $|\nabla \times \hat{\mathbf{b}}(\mathbf{x})| > u_c$. Note that $\langle \Delta\phi \rangle \sim \eta\alpha l \sim \langle E \rangle$ with l the magnetogram resolution (by unit convention, $\langle |\mathbf{B}(x,y,0)|^2 \rangle = 1$).

17 Parameter Exploration, Spectral evolution

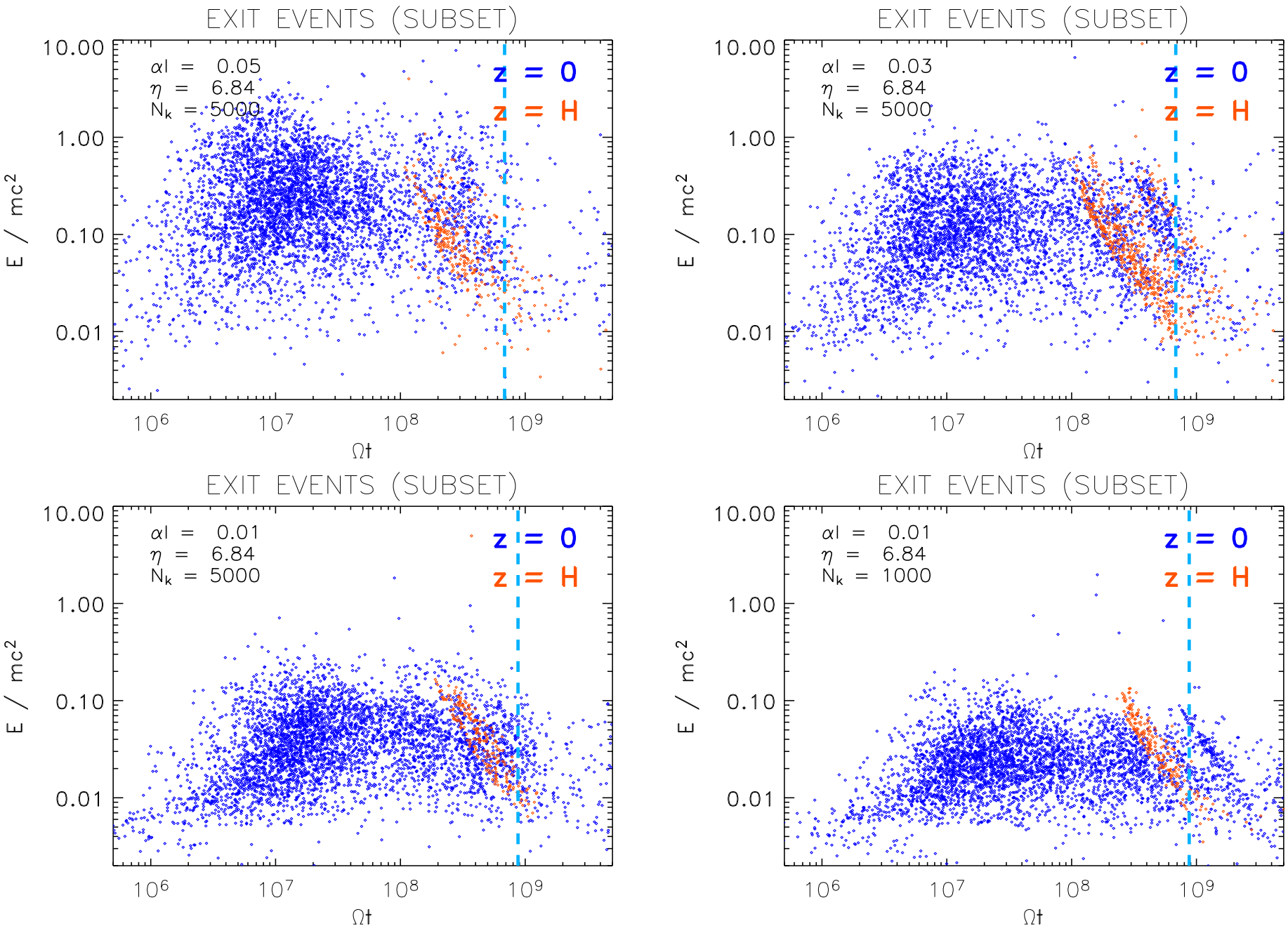

Free escape time (dashed) is $t_{\rm fe} = H/v_0$. Velocity filter at $z = H$.

18 Observations: Timing of HXR (RHESSI) and Radio (PHOENIX2)

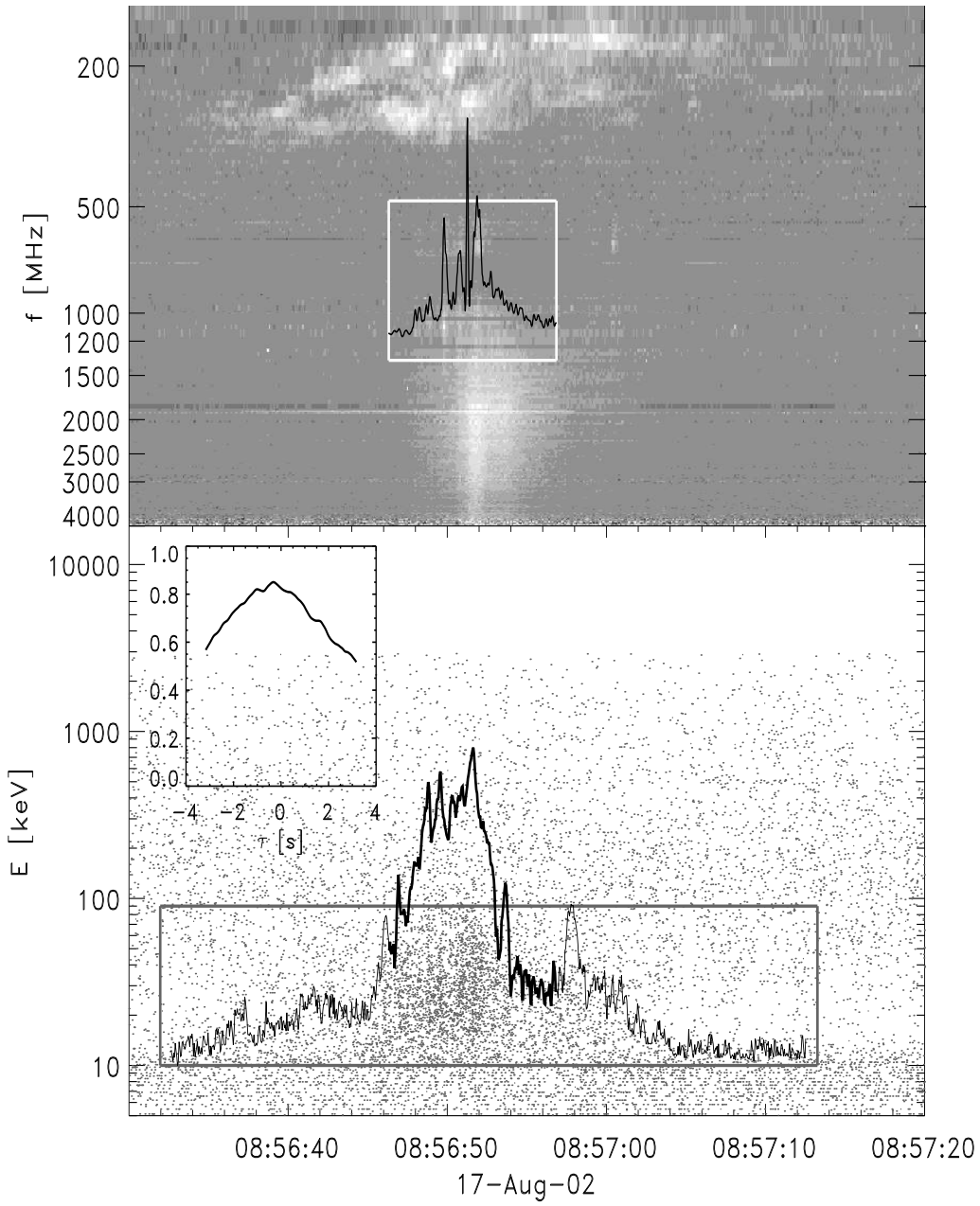

From a set of 22 correlated events (◇: normal drifting type III; △: reversed drifting type III; +: decimetric pulsations or patches) Arzner & Benz (2005) £nd:

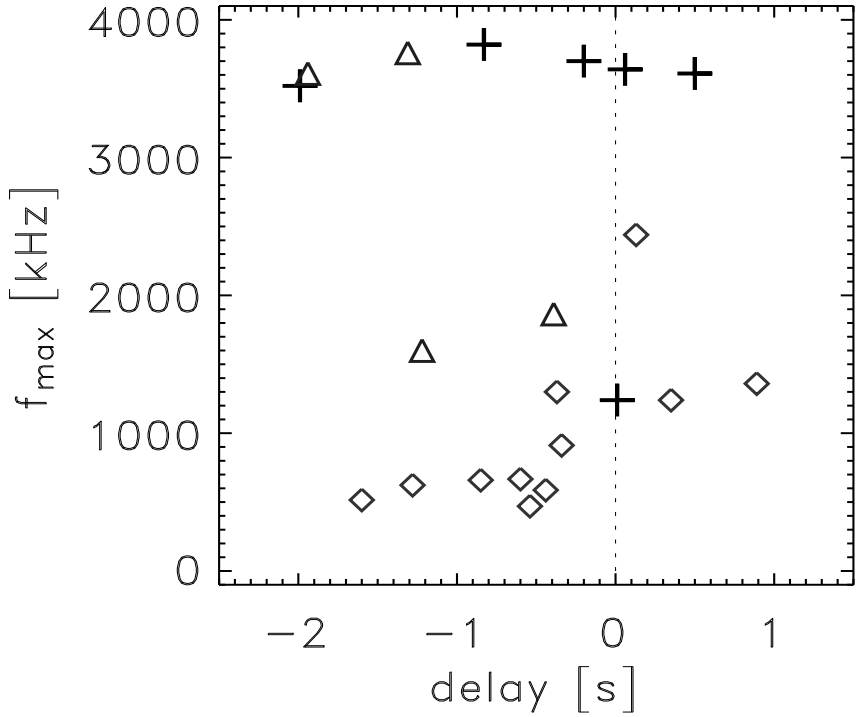

HXR typically lead the radio waves by fractions of a second.

19 Summary

Loukas and I have tried to model the global flaring process by simple test particle orbits in a slab of force-free time-independent corona with (postulated) anomaleous resistivity where the magnetic twist $\nabla \times \hat{\mathbf{b}}$ exceeds a given threshold u_c. Inside these 'dissipation regions', electrons get accelerated by the parallel electric field $\eta \mathbf{j}$; between the regions, the transport is adiabatic. The magnetic field is a constant-α force-free extrapolation from SOHO.

Electrons impacting z = 0 are associated with HXR; those escaping at $z \sim$ 50.000 km are associated with radio (type III onset), and the trapped ones with gyrosynchrotron radiation. Seeding all electrons in at t = 0 inside the dissipation regions, we find that the HXR lead the radio waves by fractions of a second, and that this finding is stable against variation of the force-free parameter αl and of the anomaleous resistivity η. The basic reason is that small scales (large twist) are concentrated at low altitudes. The rms terminal particle energy is about $\eta \alpha l$, but the detailed spectra depend on $(\eta, \alpha l, u_c l)$. Non-exponential tails may occur.

20 Appendix: Bremsstrahlung cross-section (example)